In-situ reactive synthesis of dense nanostructured β-FeSi2 by Spark Plasma Sintering

Linda Abbassi, David Mesguich, Loïc Coulomb, Geoffroy Chevallier, Romain
Aries, Claude Estournès, Emmanuel Flahaut, Romain Viennois, Mickaël
Beaudhuin

In-situ reactive synthesis of dense nanostructured β-FeSi₂ by Spark Plasma Sintering

Linda Abbassi[a,b,*], David Mesguich[b], Loïc Coulomb[a], Geoffroy Chevallier[b,c], Romain Aries[b], Claude Estournès[b], Emmanuel Flahaut[b], Romain Viennois[a], Mickaël Beaudhuin[a,*]

[a]ICGM, Univ. Montpellier, CNRS, ENSCM, Montpellier, France
[b]CIRIMAT, Université de Toulouse, CNRS, INPT, UPS, UMR CNRS-UPS-INP N°5085, Université Toulouse 3 Paul Sabatier, Bât. CIRIMAT, 118, route de Narbonne, 31062 Toulouse cedex 9, France
[c]Plateforme Nationale CNRS de Frittage Flash, PNF2, MHT, Université Toulouse 3 – Paul Sabatier, 118 route de Narbonne, F-31062 Toulouse cedex 9, France

Abstract

β-FeSi₂ is a promising material for thermoelectric application, especially if it can be nanostructured to decrease the lattice contribution to the thermal conductivity. It can be even more interesting if the entire chain of processes implemented to obtain it is not too time and energy consuming. In this paper we report a simple route to synthesize nano-β-FeSi₂ by combining mechanical milling and re- active spark plasma sintering of Fe-Si alloys. A map of the pressure-temperature conditions using a spark plasma sintering setup was performed and shows that it is possible to obtain nano-β-FeSi₂ pellets with a density above 90 % using dwell times as short as 5 min. The impact, of both, the density and nanostructuring on the hardness of the β-FeSi₂ pellets obtained by this process are presented as well as the impact of the thermoelectric properties of the materials.

Keywords: intermetallics, nanostructured materials, semiconductors, thermoelectic materials, sintering, mechanical properties

---

[*] **Corresponding author:**
Email addresses: linda.abbassi@hotmail.fr (Linda Abbassi),
mickael.beaudhuin@umontpellier.fr (Mickaël Beaudhuin)

1. Introduction

The awareness of global warming has led the scientific community to investigate new materials able to produce electricity from green resources. Thermo- electric materials (TEM) participate to this effort by converting lost heat into electricity. Their performances are linked to the Figure of Merit (Equation 1) [1]:

$$ZT = \frac{\alpha^2 \sigma}{\lambda} T \tag{1}$$

Where α is the Seebeck coefficient, σ the electrical conductivity, λ the thermal conductivity and T the temperature. Usually, thermoelectric materials are selected depending on their ZT. In the mid-temperature range 200 - 600 °C, PbTe is one of the best TEM with a ZT equal or above to 1 [2]. Nowadays, due to environmental issues, the figure of merit is no longer the only parameter to be considered and the scarcity, toxicity and cost of the chemical elements used also need to be taken into account [3]. Semiconducting intermetallic silicides can overcome these concerns as it was shown that $Mg_2(Si,Sn)$ or higher manganese silicide compounds can reach a ZT about 1.4 at 527 °C for n-type [4] and 0.9 at 427 °C for p-type [5] conducting materials respectively [6] and can be used to developed high performance TE modules [7, 8]. β-$FeSi_2$ is also a promising candidate for medium-high temperature range applications because of the abundance of Fe and Si, the low cost of these elements, its good stability and resistance to oxidation [9] as well as its optimization potential. It decomposes at 982 °C [10] to form α-Fe_2Si_5 and ε-FeSi. As described by Dusausoy *et al.* [11], β-$FeSi_2$ crystallizes in an orthorhombic structure (space group Cmcae) constituted by 48 atoms. It exhibits an experimental band gap between 0.8 eV and 0.9 eV [12, 13, 14], which is in good agreement with density functional theory (DFT) calculations [15, 16].

It also has the advantage to be easily p-type and n-type doped both with maximum ZT of 0.4 at 570 °C and of 0.2 at 577 °C, for $Fe_{0.95}Co_{0.05}Si_2$ and $FeSi_{1.92}Al_{0.08}$ respectively [17]. However, the ZT values of these compounds could be further improved if one would be able to reduce their lattice thermal conductivity (λ) which is about 4.3 $W \cdot m^{-1} \cdot K^{-1}$ and 6.2 $W \cdot m^{-1} \cdot K^{-1}$ at room temperature, respectively, without compromising their

high power factor $\alpha^2\sigma$, which is as large as the one of PbTe or Bi_2Te_3 [18, 19, 20]. To decrease λ, one strategy would be to diminish the crystallite size in order to increase the phonon scattering at the interfaces, as observed for example in $CrSi_2$ alloys [21, 22].

As the compound β-$FeSi_2$ exhibits an incongruent melting point [10, 23], several synthesis routes have been explored. A melting from the raw materials led to a mixture of the α-Fe_2Si_5 and ε-$FeSi$ phases by eutectoïd solidification. Then, through the peritectoïd transformation, α-Fe_2Si_5 and ε-$FeSi$ give β-$FeSi_2$, which is induced by the inter-diffusion between these high temperature phases.

At 937 °C, the eutectoïd decomposition reaction of α-Fe_2Si_5 conducts to the formation of β-$FeSi_2$ + Si. Finally, the reaction between ε-$FeSi$ and Si leads also to the formation of β-$FeSi_2$. The kinetics of these reactions are slow [24, 25], thus they generally occur after a long annealing time [26] which is one of the limits for the large-scale production [27, 28, 29, 30, 31].

To obtain single crystals, crystal growth techniques were used such as temperature gradient solution growth methods using metallic fluxes [32, 33] and chemical vapor transport method using iodine as gas vector [34, 35]. The needle-like shape crystals obtained by these techniques were about 5 and 10 mm respectively, and the crystal growth period varied from 72 h [33, 36] to 672 h [35, 37].

Polycrystalline sample are generally obtained from a combination of several techniques such as melting (i.e. arc furnace, induction furnace, melt spinning), powder metallurgy (i.e. mechanical milling, mechanical alloying followed by a sintering step using hot-press or spark plasma sintering) and/or annealing [26, 27, 31, 38, 39, 40, 41]. The different approaches investigated in the literature to synthesis β-$FeSi_2$ are quite time consuming, requiring from 11 h [40] to 500 h [30].

Han *et al.* [42] have shown that it is possible to obtain β-$FeSi_2$ by combining melt-spinning and SPS techniques followed by a short annealing step. Although after melt-spinning the main phases were α-Fe_2Si_5 and ε-$FeSi$ they obtained pure β-$FeSi_2$ samples after SPS and annealing, with a relative density of 98 % and a grain size ranging from

200 to 600 nm. Reactive SPS is a powerful and fast technique not only for shaping materials but also for obtaining fast solid state reaction permitting to save time and energy during the synthesis process of inorganic materials, especially in the case of incongruent materials [43, 44]. Because of its short duration, the SPS technique also enables to shape powders of nanometric size with limited grain coarsening.

In the present work, we report a process to obtain nanometric β-FeSi$_2$ dense pellets by combining mechanical milling and reactive sintering using SPS technique.

The exploration of the Pressure-Temperature SPS conditions are presented, as well as Vickers micro-hardness as a function of the relative density and the thermoelectric properties.

2. Material and methods

2.1. Sample preparation

β-FeSi$_2$ was synthesized by arc melting the elements in the stoichiometric ratio under argon (5N) atmosphere using high purity Si lump (6N) and Fe pieces (4N). The ingots obtained by this technique were first crushed in an agate mortar and then milled in a Fritsch "Pulverisette 7" planetary micromill. A container (45 ml) and 5 balls with a diameter of 15 mm, both in silicon nitride, were used as the milling media with a ball to powder ratio of 1:10. The speed of the supporting disc and of the grinding bowl was 510 rpm and 1020 rpm, respectively, for all the experiments (ball acceleration $\approx$ 80 m·s^{-2}). The milling operation was carried out inside a glove box under argon atmosphere. The sample was milled for 10 min, 30 min or 10 h.

Spark plasma sintering experiments were performed at the Plateforme Nationale CNRS de Frittage Flash located at the Université Toulouse 3, Paul Sabatier (Toulouse, France) with a Dr.Sinter 632Lx unit from Fuji Electronic Industrial CO., Japan. The milled powder was placed in 8 mm inner diameter Co-doped tungsten carbide or graphite dies for experiments up to 800 °C and 900 °C respectively. Prior to the filling of the die by the

100   powder, a graphite foil (PERMA-FOIL®Toyo Tanso) was placed on the inside wall of the die and at the interface between the punches and the powder for easy removal of the samples after the sintering cycles. Then, the samples were sintered between 500 °C to 900 °C for 5 min in a range of 50 MPa to 500 MPa as shown in the Table 2 in vacuum (residual cell

105   pressure < 5 Pa). A direct current pulse pattern of 40 ms : 7 ms (pulse on : pulse off) is used and temperature is controlled by an K-type thermocouple located on a hole (3 mm in depth) at the external surface of the die.

2.2. Sample characterization

110   The samples were analyzed by using a X-Ray Diffraction apparatus (Philips EMPYREAN with a CoKα radiation 1.78901 Å; Philips X'Pert, CuKα radiation 1.5406 Å equipped with a fast detector PW3050/60 at 45 kV and 30 mA settings. The XRD patterns were analyzed by pattern matching and Rietveld refinement using Fullprof software [45]. The

115   pellets microstructure was analyzed by Scanning Electron Microscopy (SEM) FEI Quanta 200 FEG operated at 15 kV and EDX analyses were carried out with a Silicon Drift Detector Ultim Max 100 mm^2 of Oxford Instruments.

    The relative density was determined from the density ρ measured by

120   Archimedes' method using the value of 4.93 g·cm^{-3} for the bulk phase [11].

    The electrical resistivity (Van der Pauw's method [46]) and Seebeck's coefficient were measured, in temperature, using a homemade apparatus.

    Finally, Vickers micro-hardness was measured with micro-hardness

125   testing machine Mitutoyo HM-220 with a 0.2 kg load applied during 10 s. Each hardness values given in the paper are the average of 10 measures.

3. Results and discussion

130   ### 3.1. Structural and microstructural analysis

The X-ray diffraction patterns of the powders obtained after arc melting exhibits the high temperature phases, which were α-Fe$_2$Si$_5$ and ϵ-FeSi

(Figure 1-a). The powders milled during 10 min, 30 min or 10 h are also shown in the Figure 1-a. As in the case of the material obtained directly after arc furnace, both α-Fe$_2$Si$_5$ and ε-FeSi phases can be observed in the powders milled during 10 min or 30 min whereas after 10 h of milling the β-FeSi$_2$ phase starts to appear. Such behavior was already observed by Umemoto *et al.*, when they performed a mechanical alloying of Si and Fe powders during 500 h [30]. Noticed that increasing the milling time from 10 min to 10 h leads, to peak broadening, which is inherent to a grain size refinement [21, 47].
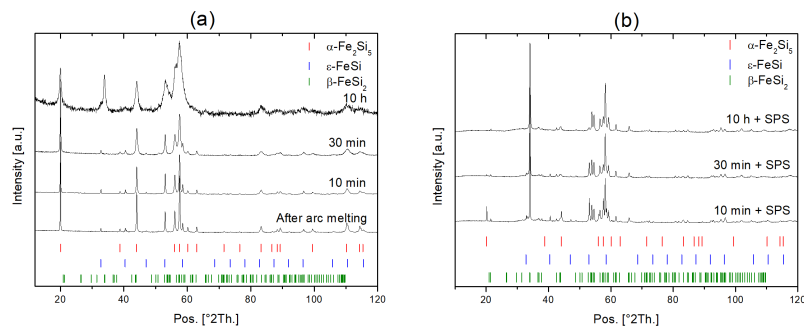

Figure 1: The X-ray diffraction patterns of : (a) the powder obtained after arc melting, the as milled powder for 10 min, 30 min or 10 h. (Nota: The diffraction pattern at 10 h, determined with Cu wavelength, was converted to fit with Co wavelength); (b) as sintered pellet from the powder milled for 10 min, 30 min or 10 h. All samples were sintered at 500MPa - 600 °C - 5 min.

The X-ray diffraction patterns of the SPS pellets densified at 500 MPa - 600 °C for 5 min from the 10 min, 30 min or 10 h milled powders are reported in Figure 1-b. The sintering at 600 °C being far below the peritectoïd transition (i.e. 982 °C) the stabilization of the β-FeSi$_2$ phase is expected. This is indeed what is observed for all three samples while the initial powder was mainly composed of α-Fe$_2$Si$_5$ and ε-FeSi phases, the pellets are mainly composed of β-FeSi$_2$ phase. Although this process can be described as a bottom-up approach with the growth of β-FeSi$_2$ grains, it looks that the microstructure of the raw powder has a strong impact on the crystallite size. Indeed, the peaks width of the pellets made of long time milled powders are broader than the sample milled for a short period, meaning that the crystallite size should be smaller.

Milling time	β-FeSi$_2$	α-Fe$_2$Si$_5$	ε-FeSi	Si	Crystallite size

	(wt. %)	(wt. %)	(wt. %)	(wt. %)	(nm)
10 min	77	11	10	2	> 1000
30 min	90	1	7	2	> 1000
10 h	> 99	< 1	< 1	< 1	≈134

Table 1: : Evolution of the amount of β-FeSi$_2$, α-Fe$_2$Si$_5$, ε-FeSi, Si and crystallite size in SPS pellets obtained from powder milled for different times and sintered at 500 MPa – 600 °C - 5 min.

165 From the Rietveld refinement analysis of these data (see Table 1), one can observe that the amount of β-FeSi$_2$ phase increases while increasing the milling time. One can note that after SPS densification at 600 °C of the powder milled 10 min, the β-FeSi$_2$ phase is already obtained in a large amount (above 70 %) whereas the reaction tends to be more and more

170 complete on powders obtained with increased milling time. It is well known that mechanical milling induces a decrease of both the aggregate size and the crystallite size [21, 48], which is then favorable to obtain better mixing of the elements and/or higher reactivity of the phases. The main difference between our results and those of Han *et al.* [42] is the

175 crystallite size of β-FeSi$_2$ after SPS which is about 134 nm in our case, instead of 200 - 600 nm in their work.
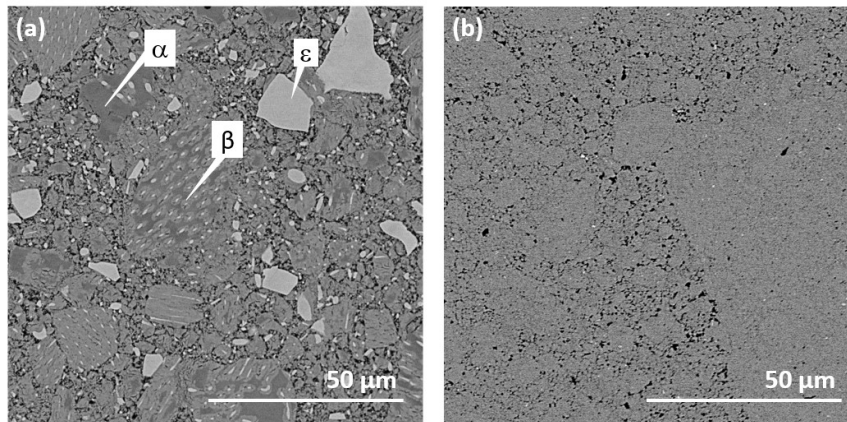
Figure 2: SEM image (backscattered electron detector) of samples sintered at 600 °C - 500 MPa - 5 min. (a) 10 min milling time; (b) 10 h milling time. α-Fe$_2$Si$_5$ appears in dark grey,
180 β-FeSi$_2$ in grey and ε-FeSi in light grey.

From the SEM image of the SPS pellets made with 10 min milled powder (see Figure 2-a) one can first confirm that most of this sample is made of β-FeSi$_2$ as observed by XRD. One can also observe on large grains an

incomplete reaction where ε-FeSi fibers are surrounded by β-FeSi$_2$ in α-Fe$_2$Si$_5$ matrix, this observation is typical of a peritectoïd reaction, the compositions were confirmed by EDX analysis. As observed in the Figure 2-b, 10 h of powder milling leads to a complete reaction to form β-FeSi$_2$. One can note that it is made of tiny grains, which was confirmed by the determination of the crystallite size owing Le Bail refinement (See Table 2).

Sample ID	T (°C)	t (min)	P (MPa)	Relative density (%)	Crystallite size (nm)
1	500	5	100	67.8	≈77
2	600	5	100	78.0	≈78
3	600	5	500	91.6	≈134
4	700	5	100	86.0	≈160
5	800	5	50	92.4	nd
6	800	5	500	95.1	nd
7	900	5	100	90.7	-

Table 2: SPS parameters, relative density and crystallite size for samples 1 to 7 (milling time 10 h). *nd: not determined.
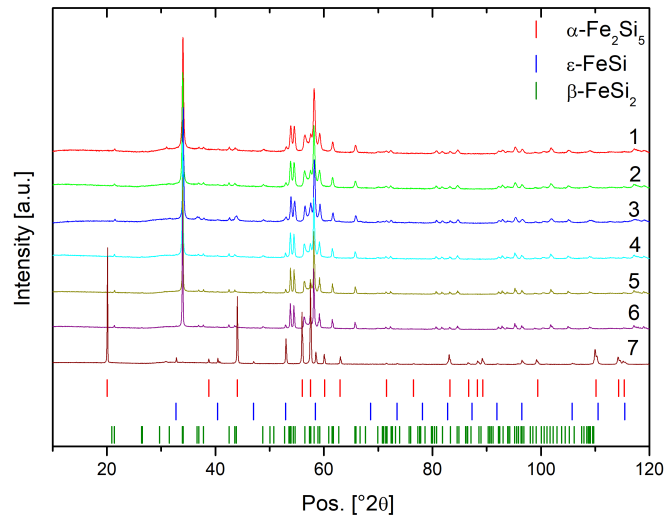
Figure 3: The X-ray diffraction patterns of pellets synthesized by SPS from milled powder for 10 hours. The sintering time was 5 min for all samples.

As 10 h of milling led to the highest amount of β-FeSi$_2$ we chose this raw powder to investigate the P-T SPS conditions to obtain β-FeSi$_2$ (see Figure 3). The sintering parameters as well as the relative density of the pellets and the crystallite size are given in Table 2.
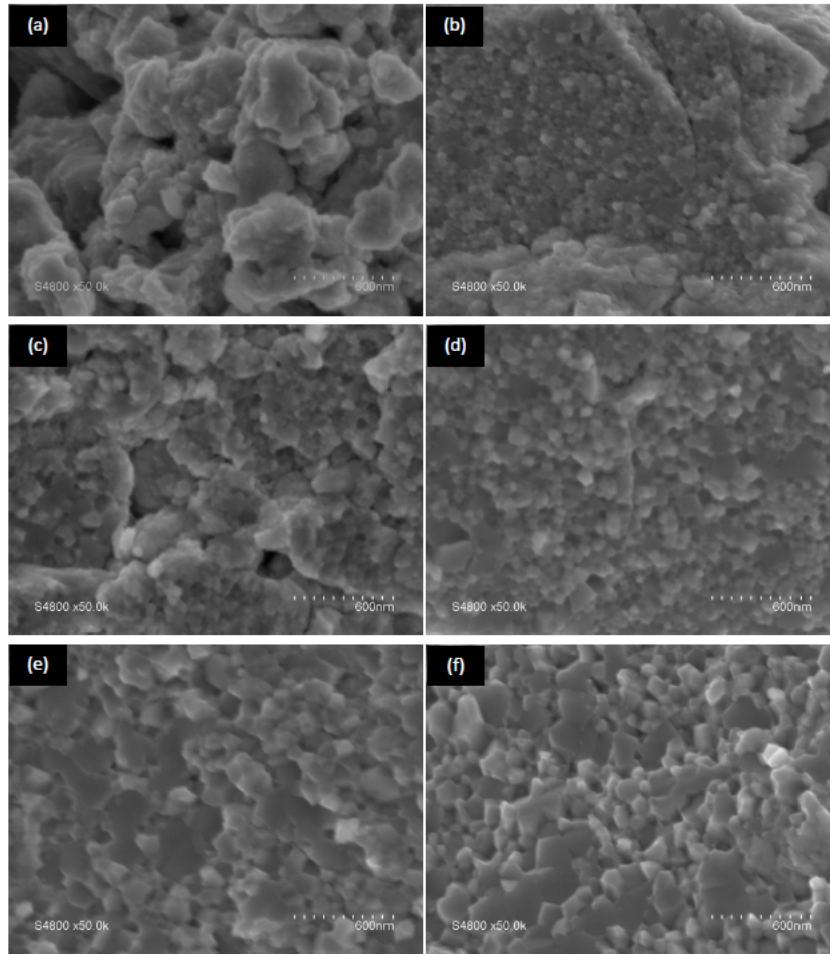

Figure 4: SEM images (fractures) of samples (a) 1, (b) 2, (c) 3, (d) 4, (e) 5 and (f) 6.

However, for samples 5 and 6, the crystallite size was not determined by refinement. The Figure 4 shows the microstructure of fractures of sample 1 to 6. In the Figures 4-a and 4-b, it is not easy to determine the crystallite size due to the resolution limit of the device. However, the modification of the SPS conditions has an effect on the grain size. Sample 6, which was synthesized at high temperature (800 °C) and high pressure (500 MPa) presents a larger grain size than sample 1 (500 °C - 100 MPa). Thus, by decreasing the sintering temperature and/or pressure, from sample 6 to sample 1 (Figure 4-f to 4-a, respectively) a limitation of the grain growth is observed, with a maximum grain size around 250 nm - 350

nm. This behavior was expected and shows that it is possible to control the

215   microstructure of β-FeSi$_2$ during the SPS process.

Our investigation shows that it is possible to obtain the phase β-FeSi$_2$ on a large P-T range (see sample 1 to 6 in Table 2). Meanwhile, α-Fe$_2$Si$_5$ and ε-FeSi are identified in large amount for the sample 7. This result is not surprising as the peritectoïd transition is at about 982 °C and that it is

220   well known that the temperature in SPS experiment is usually underestimated (tens of degrees) due to the temperature gradient in the matrix mainly due to contact resistances as evidenced from Thermo-Electric finite element modeling of the SPS process [49, 50].

To enhance the reading of the evolution of the relative density versus

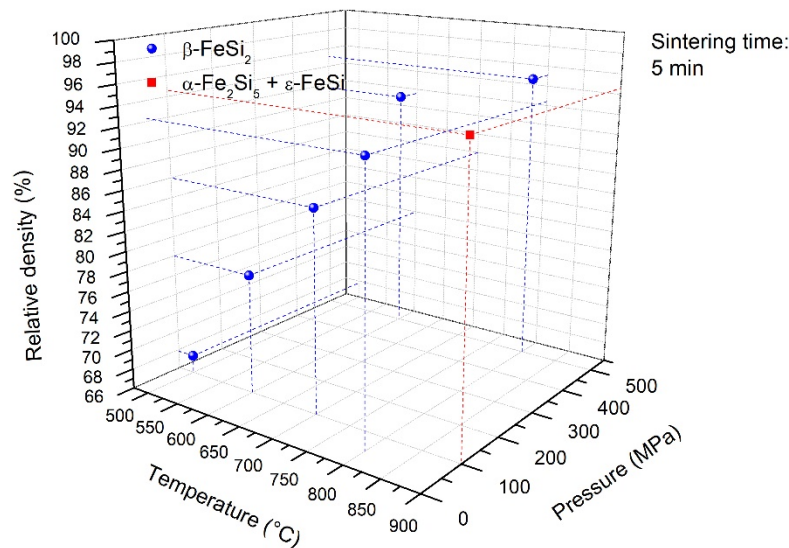225   the sintering condition, a 3D-plot is given in Figure 5.

Figure 5: Relative density given depending on SPS conditions using 10 h milled raw powder.

As expected one can observe that increasing the temperature and/or increasing the pressure leads to an increase in the pellets density. It is

230   interesting to note that the synthesis of β-FeSi$_2$ is possible, with a dwell time of only 5 min, in a low temperature regime ranging from 500 °C and up to 800 °C under an uniaxial pressure applied from 50 MPa up to 500 MPa. However, it is noteworthy that the relative density of the samples synthesized at a temperature below 700 °C and under 100 MPa is lower

235   than 90 %. Nevertheless, if the pressure is increased to 500 MPa, the relative density is higher than 90 % even for a temperature as low as 600

°C. By limiting the maximum temperature reached during the sintering, it is also possible to limit the grain coarsening, which is then favorable to maintain a nanometric size of the crystallites.
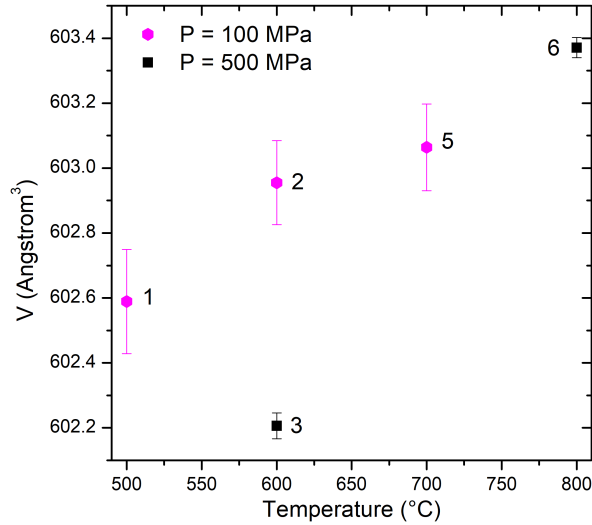
240

Figure 6: Variation of β-FeSi$_2$ volume cell for bulk samples 1, 2 and 4 sintered at 500 °C, 600 °C and 700 °C, respectively. Pressure applied was 100 MPa and dwell time was 5 min for all samples. Samples 3 and 5 were sintered at 600 °C and sample 4 at 800 °C. Pressure applied was 500 MPa and dwell time was 5 min.

245   In Figure 6 we report the variation of the volume cell for the samples sintered at P = 100 MPa and for different sintering temperatures. As described by Wappling *et al.*, the cell parameters are: a = 9.8795(5) Å; b = 7.7977(3) Å; c = 7.8392(3) Å with a volume of V = 603.2 Å^3 for a sample annealed at 900 °C during 6 days [51]. With increasing the temperature,

250   one notes the increase in the volume cell until V = 603.0(1) Å^3 for sintering temperature of 700 °C, which is in good agreement with Wappling's value [51]. Thus, this behavior can be explained by the process used to obtain the pellets. Indeed, it is well known that mechanical milling and SPS induce microstrains [52]. Consequently, increasing the sintering

255   temperature led to a relaxation of the unit cell to the experimental value of bulk or long time annealed β-FeSi$_2$ samples.

3.2. Mechanical properties

The Vickers Hardness (HV) values versus the relative density is reported in the Figure 7. The HV value (in GPa) was calculated by the following formula:

$$HV = \frac{2F \times \sin\left(\frac{136}{2}\right)}{d^2} = 1.8 \times \frac{F}{d^2}$$

with F (in N) the force applied during 10 s and d the mean of diagonal indentations (in mm). The Vickers micro hardness could not be measured for the sample 1 due to its high porosity rate.
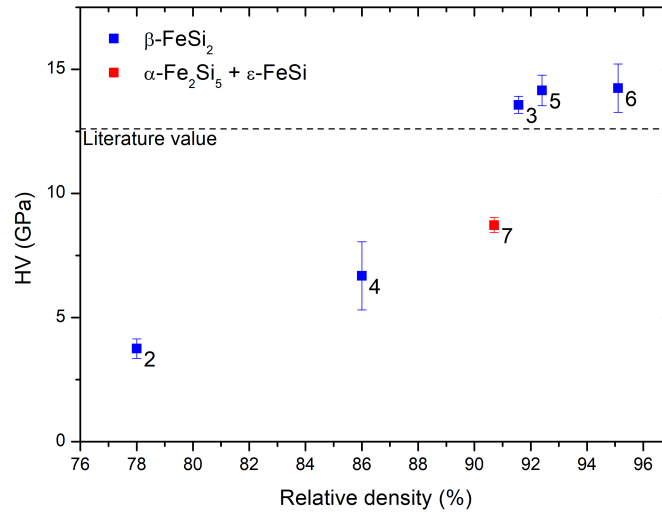

Figure 7: Vickers micro hardness versus the relative density of samples presented in Table 2. Blue circles: β-FeSi$_2$, red square: α-Fe$_2$Si$_5$ + ε-FeSi. The dashed line represents the HV literature value of β-FeSi$_2$ [53].

As expected, the HV value increases with increasing the density from 78 % to 92 % from 3.7(4) GPa to a plateau of 14(1) GPa respectively. The plateau value is slightly higher than the maximum value of HV found for β-FeSi$_2$ in the literature (12.6 GPa [53]). The larger value that we find could be explained by the decrease in the crystallite size as explained by Naik *et al.* following the Hall-Petch relationship [54] and by a rather high relative density (higher than 92 %).

At the opposite, the sample 7 exhibits a low HV value of 8.7(3) GPa which was expected as it is composed of a mixture of the α-Fe$_2$Si$_5$ + ε-FeSi phases. For these compounds, Milekhine *et al.* [55] found a HV values equal to 5.6 GPa and 9.3 GPa for α-Fe$_2$Si$_5$ and ε-FeSi respectively,

which explains the decreased HV value for the sample 7 despite its quite high relative density (> 90 %).

3.3. Thermoelectric properties

285   Electronic properties were measured for all samples composed of β-FeSi$_2$ phase. The Figure 8-a reveals a positive Seebeck coefficient for all samples, which is a characteristic of a conduction dominated by holes and then of p-type semi-conductors. Depending on the sintering conditions, a variation of the maximum Seebeck coefficient is observed from ≈ 45

290   μV·K^{-1} to ≈ 85 μV·K^{-1}.

Moreover, a shift in the temperature of the maximum of the Seebeck coefficient is observed. In Figure 8-a, when the density of the pellets increases, from sample 1 to sample 5, one can note a shift of the maximum, from α_1 = 59.3 μV·K^{-1} at T = 400 °C to α_5 = 70.8 μV·K^{-1} at T = 300 °C

295   respectively, toward lower temperatures. This behavior can be explained by a change from extrinsic to intrinsic conduction which is characteristic of a change from heavily doped to lightly doped semi-conductor [40]. This could be assimilated to an increase in defects in the samples sintered at lower temperature. However, the trend changes for sample 6 which was

300   sintered at both higher pressure (500 MPa) and temperature (800 °C). One can also note that sample 6 exhibits the lowest Seebeck coefficient but compared to sample 2, which was sintered at the same pressure, there is no significant change in temperature of the maximum of the Seebeck coefficient. This behavior could be explained by the different types of

305   defects which are present in β-FeSi$_2$ and which could modify the carrier concentration and lower the Seebeck coefficient [56].
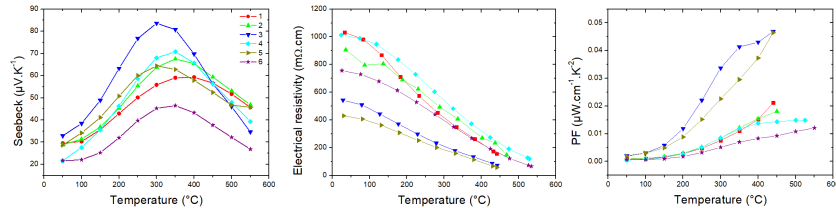
Figure 8: Thermoelectric properties of β-FeSi$_2$ sintered at different temperature and pressure and given in Table 2. (a) Seebeck coefficient, (b) Electrical resistivity and (c)
310   Power Factor (PF).

The Figure 8-b presents the decrease in the electrical resistivity of these samples with the temperature, which is typical of a semi-conductor. In addition, samples 1, 2 and 4 exhibit a high electrical resistivity at low temperature, around 1000 mΩ·cm, due to their high porosity rate. By increasing the pressure to 500 MPa and/or the temperature we observed that the electrical resistivity decreased drastically (sample 3, 5 and 6) until around 430 mΩ·cm for the sample 5. Commonly, increasing the sintering temperature leads to an increase in the grain coarsening [57] and then to a decrease of the electrical resistivity. It can be noticed that sample 6 does not follow this trend, as mentioned for the Seebeck coefficient.

The power factor (PF) is plotted versus the temperature in Figure 8-c and shows that samples with a higher porosity rate exhibit a smaller PF than dense samples (3 and 5). The maximum value of the PF was 0.05 $\mu W \cdot cm^{-1} \cdot K^{-2}$ for samples 3, which was sintered at 600 °C and 500 MPa. Its microstructure exhibits a crystallite size around 134 nm and its relative density is 91.6 %. Thus, the increase of PF value is mainly due to high Seebeck coefficient reached owing the nanostructuring on β-FeSi$_2$.

4. Conclusions

This investigation shows that nanostructured β-FeSi$_2$ can be synthesized by reactive SPS from Fe-Si alloys after a thorough mixing by mechanical milling. We also show that increasing the milling time is favorable to obtain finely mixed α-Fe$_2$Si$_5$ and ε-FeSi powders transformed and densified into bulk samples of β- FeSi$_2$ by reactive SPS. A large P-T domain was identified to obtain this phase however one can note that the conditions 600 °C - 500 MPa - 5 min are a good compromise to obtain dense pellets while maintaining a small crystallite size of only 134 nm. The mechanical characterization has shown that the nano crystal- lite size of the pellets enhanced the Vickers micro-hardness. The thermoelectric characterization also showed that this sample had the best power factor as it had the highest Seebeck coefficient. This study opens the route to multi-scale investigation of β-FeSi$_2$ alloys combining optimized carrier concentration and nanostructuring to enhance the figure of merit.

        References

        [1] H. J. Goldsmid, Thermoelectric Refrigeration, Springer US, Boston,
            MA, 1964.

355   [2] D. M. Rowe, Thermoelectrics Handbook: Macro to Nano,
            CRC/Taylor & Francis, 2006.

        [3] S. LeBlanc, S. K. Yee, M. L. Scullin, C. Dames, K. E. Goodson,
            Material and manufacturing cost considerations for thermoelectrics,
            Renewable and Sustainable Energy Reviews 32 (2014) 313–327.

360   [4] A. Khan, N. Vlachos, T. Kyratsi, High thermoelectric figure of merit
            of Mg2Si0.55Sn0.4Ge0.05 materials doped with Bi and Sb, Scripta
            Materialia 69 (8) (2013) 606–609.

        [5] D. M. Rowe, CRC Handbook of Thermoelectrics, CRC Press,
            1995.

365   [6] M. I. Fedorov, G. N. Isachenko, Silicides: Materials for
            thermoelectric energy conversion, Japanese Journal of Applied
            Physics 54 (7S2) (2015) 07JA05.

        [7] H. Ihou Mouko, K. Romanjek, M. Mejri, M. Oulfarsi, S. El
            Oualid, P. Malinconi, Y. Thimont, B. Malard, C. Estournès, N.
370   David, A. Dauscher, Manufacturing and performances of
            silicide-based thermoelectric modules, Energy Conversion and
            Management 242 (2021) 114304.

        [8] G. Skomedal, L. Holmgren, H. Middleton, I. Eremin, G.
            Isachenko, M. Jaegle, K. Tarantik, N. Vlachos, M. Manoli, T.
375   Kyratsi, D. Berthebaud, N. Y. Dao Truong, F. Gascoin, Design,
            assembly and characterization of silicide- based thermoelectric
            modules, Energy Conversion and Management 110 (2016) 13–
            21.

380 [9] M. Nanko, S. H. Chang, K. Matsumaru, K. Ishizaki, M. Takeda, Isothermal oxidation of sintered β-FeSi$_2$ in air, Materials Science Forum 522-523 (2006) 641–648.

[10] O. K. von Goldbeck, Fe—Si Iron—Silicon, in: IRON—Binary Phase Diagrams, Springer Berlin Heidelberg, Berlin,
385 Heidelberg, 1982, pp. 136–139.

[11] Y. Dusausoy, J. Protas, R. Wandji, B. Roques, Structure cristalline du disiliciure de fer, FeSi$_2\beta$, Acta Crystallographica Section B Structural Crystallography and Crystal Chemistry 27 (6) (1971) 1209–1218.

390 [12] R. Ware, D. McNeill, Iron disilicide as a thermoelectric generator material, Proceedings of the Institution of Electrical Engineers 111 (1) (1964) 178.

[13] S. Eisebitt, J. E. Rubensson, M. Nicodemus, T. Boske, S. Blügel, W. Eberhardt, K. Radermacher, S. Mantl, G. Bihlmayer,
395 Electronic structure of buried α-FeSi$_2$ and β-FeSi$_2$ layers: Soft-x-ray-emission and -absorption studies compared to band-structure calculations, Physical Review B 50 (24) (1994) 18330–18340.

[14] D. J. Oostra, C. W. T. Bulle-Lieuwma, D. E. W. Vandenhoudt,
400 F. Felten, J. C. Jans, β-FeSi$_2$ in (111) Si and in (001) Si formed by ion-beam synthesis, Journal of Applied Physics 74 (7) (1993) 4347–4353.

[15] J. Chai, C. Ming, X. Du, P. Qiu, Y. Y. Sun, L. Chen, Thermodynamics, kinetics and electronic properties of point
405 defects in β-FeSi$_2$, Physical Chemistry Chemical Physics 21 (20) (2019) 10497–10504.

[16] N. E. Christensen, Electronic structure of β-FeSi$_2$, Physical Review B 42 (11) (1990) 7148–7153.

[17] J. Hesse, Leistungsthermoelemente aus Eisendisilicid fur die
410 Stromerzeugung, Zeitschrift fur Angewandte Physik 28 (1969) 133.

[18] A. Heinrich, G. Behr, H. Griessmann, S. Teichert, H. Lange, Thermopower, Electrical and Hall Conductivity of Undoped and Doped Iron Disilicide Single Crystals, MRS Proceedings 478
415 (1997) 255.

[19] B. Paul, A. K. V, P. Banerji, Embedded Ag-rich nanodots in PbTe: Enhancement of thermoelectric properties through energy

filtering of the carriers, Journal of Applied Physics 108 (6) (2010) 064322.

[20] M.-K. Han, Y. Jin, D.-H. Lee, S.-J. Kim, Thermoelectric Properties of Bi_2Te_3: CuI and the Effect of Its Doping with Pb Atoms, Materials 10 (11) (2017) 1235.

[21] M. Khalil, A. Moll, M. Godfroy, A. Letrouit-Lebranchu, B. Villeroy, E. Alleno, R. Viennois, M. Beaudhuin, Thermoelectric properties and stability of nanostructured chromium disilicide $CrSi_2$, Journal of Applied Physics 126 (13) (2019) 135103.

[22] A. Moll, R. Viennois, M. Boehm, M. M. Koza, Y. Sidis, J. Rouquette, S. Laborde, J. Debray, B. Menaert, J.-P. Castellan, C. Candolfi, B. Lenoir, P. Hermet, M. Beaudhuin, Anharmonicity and Effect of the Nanostructuring on the Lattice Dynamics of $CrSi_2$, The Journal of Physical Chemistry C 125 (27) (2021) 14786–14796.

[23] S. Cui, I.-H. Jung, Critical reassessment of the Fe-Si system, Calphad 56 (2017) 108–125.

[24] T. Sakata, Y. Sakai, H. Yoshino, H. Fujii, I. Nishida, Studies on the formation of $FeSi_2$ from the $FeSi$-Fe_2Si_5 eutectic, Journal of the Less Common Metals 61 (2) (1978) 301–308.

[25] B. I. Nishida, K. Masumoto, T. Kojima, Formation of $FeSi_2$ from sintered $FeSi$-Fe_2Si_5 Eutectic alloy, Transactions of the Japan Institute of Metals 26 (5) (1985) 369–374.

[26] H. Takizawa, P. F. Mo, T. Endo, M. Shimada, Preparation and thermoelectric properties of β-$Fe_{1-x}Ru_xSi_2$, Journal of Materials Science 30 (16) (1995) 4199–4203.

[27] Y. Ohta, S. Miura, Y. Mishima, Thermoelectric semiconductor iron disilicides produced by sintering elemental powders, Intermetallics 7 (11) (1999) 1203–1210.

[28] K. Lefki, P. Muret, E. Bustarret, N. Boutarek, R. Madar, J. Chevrier, J. Derrien, M. Brunel, Infrared and Raman characterization of beta iron silicide, Solid State Communications 80 (10) (1991) 791–795.

[29] N. Nakatsuka, H. Yasuda, T. Nagira, M. Yoshiya, Three-dimensional alignment of $FeSi_2$ with orthorhombic symmetry by an anisotropic magnetic field, Journal of Physics: Conference Series 165 (2009).

455   [30] M. Umemoto, Preparation of Thermoelectric β-FeSi₂ Doped with Al and Mn by Mechanical Alloying (Overview), Materials Transactions, JIM 36 (2) (1995) 373–383.

[31] J. ichi Tani, H. Kido, Thermoelectric properties of Pt-doped β-FeSi₂, Journal of Applied Physics 88 (10) (2000) 5810–5813.

460   [32] H. Kannou, Y. Saito, M. Kuramoto, T. Takeyama, T. Nakamura, T. Matsuyama, H. Udono, Y. Maeda, M. Tanaka, Z. Liu, H. Tatsuoka, H. Kuwabara, Structural and electrical properties of β-FeSi₂ single crystals grown using Sb solvent, Thin Solid Films 461 (1) (2004) 110–115.

465   [33] H. Udono, I. Kikuma, Electrical properties of p-type β-FeSi₂ single crystals grown from Ga and Zn solvents, Thin Solid Films 461 (1) (2004) 188–192.

[34] G. Behr, J. Werner, G. Weise, A. Heinrich, A. Burkov, C. Gladun, Preparation and Properties of High-Purity β-FeSi₂
470   Single Crystals, physica status solidi (a) 160 (2) (1997) 549–556.

[35] J. Wang, S. Saitou, S. Ji, M. Isshiki, Growth conditions of β-FeSi₂ single crystals by chemical vapor transport, Journal of Crystal Growth 295 (2) (2006) 129–132.

475   [36] G. Guizzetti, F. Marabelli, M. Patrini, P. Pellegrino, B. Pivac, L. Miglio, V. Meregalli, H. Lange, W. Henrion, V. Tomm, Measurement and simulation of anisotropy in the infrared and Raman spectra of β-FeSi₂ single crystals, Physical Review B 55 (21) (1997) 14290–14297.

480   [37] K. Gotoh, H. Suzuki, H. Udono, I. Kikuma, F. Esaka, M. Uchikoshi, M. Isshiki, Single crystalline β-FeSi₂ grown using high-purity FeSi₂ source, Thin Solid Films 515 (22) (2007) 8263–8267.

[38] K. Lefki, P. Muret, E. Bustarret, N. Boutarek, R. Madar, J.
485   Chevrier, J. Derrien, M. Brunel, Infrared and Raman characterization of beta iron silicide, Solid State Communications 80 (10) (1991) 791–795.

[39] S. W. Kim, M. K. Cho, Y. Mishima, D. C. Choi, High temperature thermoelectric properties of p- and n-type β-FeSi₂
490   with some dopants, Intermetallics 11 (5) (2003) 399–405.

[40] M. Ito, H. Nagai, T. Tahata, S. Katsuyama, K. Majima, Effects of Zr substitution on phase transformation and thermoelectric

properties of β-FeSi$_2$, Journal of Applied Physics 92 (6) (2002) 3217–3222.

[41] H. Wu, B. Hu, N. Tian, Q. Zheng, Preparation of β-FeSi$_2$ thermoelectric material by laser sintering, Materials Letters 65 (19-20) (2011) 2877–2879.

[42] L. Han, T. Xin-Feng, C. Wei-Qiang, Z. Qing-Jie, Quick preparation and thermal transport properties of nanostructured β-FeSi$_2$ bulk material, Chinese Physics B 18 (1) (2009) 287–292.

[43] Z. A. Munir, U. Anselmi-Tamburini, M. Ohyanagi, The effect of electric field and pressure on the synthesis and consolidation of materials: A review of the spark plasma sintering method, Journal of Materials Science 41 (3) (2006) 763–777.

[44] C. Estournès, Mise en forme de matériaux par frittage flash, Techniques de l'ingénieur 33 (0) (2006) IN 56.

[45] J. Rodriguez-Carvajal, Fullprof: a program for rietveld refinement and pattern matching analysis, in: satellite meeting on powder diffraction of the XV congress of the IUCr, Toulouse, France, 1990, p. 127.

[46] L. J. ven der Pauw, A method of measuring specific resistivity and hall effect of discs of arbitrary shape, Philips Res. Rep 13 (1) (1958) 1–9.

[47] M. Khalil, M. Beaudhuin, B. Villeroy, D. Ravot, R. Viennois, A modeling approach for new CrSi$_2$ based alloys: Application to metastable Cr$_{1-x}$Zr$_x$Si$_2$ as a potential thermoelectric material, Journal of Alloys and Compounds 662 (2016) 150–156.

[48] S. Karuppaiah, M. Beaudhuin, R. Viennois, Investigation on the thermoelectric properties of nanostructured Cr$_{1-x}$Ti$_x$Si$_2$, Journal of Solid State Chemistry 199 (2013) 90–95.

[49] A. Pavia, L. Durand, F. Ajustron, V. Bley, G. Chevallier, A. Peigney, C. Estournès, Electro-thermal measurements and finite element method simulations of a spark plasma sintering device, Journal of Materials Processing Technology 213 (8) (2013) 1327–1336.

[50] C. Manière, A. Pavia, L. Durand, G. Chevallier, K. Afanga, C. Estournès, Finite-element modeling of the electro-thermal contacts in the spark plasma sintering process, Journal of the European Ceramic Society 36 (3) (2016) 741–748.

[51] R. Wappling, L. Haggstrom, S. Rundqvist, The space group symmetry of β-FeSi$_2$ as determined by Mossbauer spectroscopy, Chemical Physics Letters 2 (3) (1968) 160–161.

[52] M. Longhin, R. Viennois, D. Ravot, J.-J. Robin, P. Papet, Nanostructuration of CoSi by mechanical milling and mechanical alloying, Solid State Sciences 38 (2014) 129–137.

[53] K. Maex, M. V. Rossum, Properties of metal silicides, INSPEC, London, 1995.

[54] S. N. Naik, S. M. Walley, The Hall–Petch and inverse Hall–Petch relations and the hardness of nanocrystalline metals, Journal of Materials Science 55 (7) (2020) 2661–2681.

[55] V. Milekhine, M. Onsøien, J. Solberg, T. Skaland, Mechanical properties of FeSi (ε), FeSi$_2$ ($\zeta\alpha$) and Mg$_2$Si, Intermetallics 10 (8) (2002) 743–750.

[56] S. Le Tonquesse, Z. Verastegui, H. Huynh, V. Dorcet, Q. Guo, V. Demange, C. Prestipino, D. Berthebaud, T. Mori, M. Pasturel, Magnesiore- duction Synthesis of Co-Doped β-FeSi$_2$: Mechanism, Microstructure, and Improved Thermoelectric Properties, ACS Applied Energy Materials 2 (12) (2019) 8525–8534.

[57] M. Shahedi Asl, A. Sabahi Namini, A. Motallebzadeh, M. Azadbeh, Effects of sintering temperature on microstructure and mechanical properties of spark plasma sintered titanium, Materials Chemistry and Physics 203 (2018) 266–273.